NÖHÜ Müh. Bilim. Derg. / NOHU J. Eng. Sci., 2023; 12(3), 950-956

Niğde Ömer Halisdemir Üniversitesi Mühendislik Bilimleri Dergisi
Niğde Ömer Halisdemir University Journal of Engineering Sciences

Araştırma makalesi / Research article

www.dergipark.org.tr/tr/pub/ngumuh / www.dergipark.org.tr/en/pub/ngumuh

Design and stress analysis of wider lateral lumbar interbody fusion (LLIF) cages: A finite element study

Daha geniş lateral lumbar interbody füzyon (LLIF) kafeslerinin tasarımı ve stres analizi: Bir sonlu eleman çalışması

Meltem Eryildiz[1,*]

[1] *Beykent University, Department of Mechanical Engineering, 34398, Istanbul, Türkiye*

Abstract

It is important to better understand the impact of intervertebral cage material and design on the stress distribution in vertebral bodies to aid eliminate complications like subsidence and improve performance after lumbar interbody fusion. In this study, the cage materials of PLA, PEEK, titanium, and stainless steel were compared using a finite element model of the L3-L4 motion segment. Strain and stress were measured in the vertebra and cage when the model was loaded in axial compression, flexion, and torsion. Additionally, a wider cage designed to conform to the vertebral endplates could potentially evenly distribute and reduce the overall stress at the endplates. The wider cages increased the area in contact with the bone, distributing the stress more evenly and providing a potential way to decrease the danger of subsidence. Such cages could be manufactured by additive manufacturing.

Keywords: Spinal cage, 3D design, Interbody fusion, FEM, Finite element, LLIF cage

Öz

Lateral Lumbar Interbody Füzyon operasyonu sonrası çökme gibi komplikasyonları ortadan kaldırmaya ve performansı artırmaya yardımcı olmak için intervertebral kafes malzemesinin ve tasarımının omur gövdelerindeki stres dağılımı üzerindeki etkisini daha iyi anlamak oldukça önemlidir. Bu çalışmada PLA, PEEK, titanyum ve paslanmaz çelik kafes malzemeleri, L3-L4 omur segmentinin sonlu elemanlar modeli kullanılarak karşılaştırılmıştır. Model eksenel bası, eğme ve dönme momentinde yüklendiğinde omur ve kafeste gerinim ve gerilim değerleri ölçülmüştür. Ayrıca, vertebral plakalara uyacak şekilde tasarlanmış daha geniş bir kafes, potansiyel olarak plakalardaki genel gerilimi eşit şekilde dağıtabilir ve azaltabilir. Daha geniş kafesler, kemikle temas halindeki alanı arttırarak, stresi daha eşit dağıtmıştır ve çökme tehlikesini azaltmak için potansiyel bir yol sağlamıştır. Bu tür kafesler eklemeli imalat ile üretilebilir.

Anahtar kelimeler: Omur kafesi, 3B tasarım, Vücutlar arası füzyon, FEM, Sonlu elemanlar, LLIF kafes

1 Introduction

Patients experience spinal injuries more frequently as a result of accidents or improper athletic activity positions. One of the most frequent injuries is the loss or reduced function of the spinal disc, which supports the spine and maintains foraminal height. The patient's mobility may be hampered by degenerative lumbar spinal stenosis, which is caused by this damage and narrowing of the spinal canal [1]. The first line of treatment is conservative; however, when conservative care fails to relieve a patient's symptoms, surgery is recommended, depending on the degree of the degenerating cervical disc [2].

Treatment for a number of spinal diseases frequently involves lumbar interbody fusion (LIF). This method avoids the need to damage the posterior spinal column while also enabling wide disc space exposure for the implantation of a large interbody graft, faster surgery times, reduced blood loss, and indirect decompression of neurological tissue [3]. Good to outstanding clinical results and few surgical risks are achieved with this technic in terms of stabilization and robust spinal fusion. In this LIF surgery, a cage between two vertebrae is implanted and filled with bone or a bone substitute to enable this fusion. The cage's subsidence and potential post-surgical cage migration are its principal drawbacks. These two factors are influenced by the cage's design and material characteristics. This operation is still widely used today despite technical advancements over the years, therefore enhancing fusion rates and clinical outcomes will require alterations to implant design and material [2, 4] Cages need to be strong enough to withstand the lumbar spine's in vivo loads. These implants should also have enough surface area to prevent disc height loss after surgery and to resist subsidence into the vertebral bodies [5].

For LIF surgeries, there are four primary surgical strategies (Figure 1). The tough decision of which surgical technique to choose for the spine is frequently influenced by the definite diagnosis, the surgeon's training, and/or their prior expertise with a certain approach. ALIF cages often best match the overall footprint of the vertebral body because this method allows access to the disc area. The medial-lateral (M-L) dimension of LLIF cages can be significantly larger than ALIF cages, allowing the implant to rest on the lateral portions of the apophyseal ring. LLIF cages are narrower than ALIF cages in the anterior-posterior (A-P) dimension.

* Sorumlu yazar / Corresponding author, e-posta / e-mail: meltemeryildiz@beykent.edu.tr (M. Eryıldız)
Geliş / Recieved: 06.02.2023 Kabul / Accepted: 23.05.2023 Yayımlanma / Published: 15.07.2023
doi: 10.28948/ngmuh.1248442

PLIF cages typically have the smallest footprints. However, they are designed to be used in pairs. TLIF cages are usually curved to match the anterior form of the vertebral body and are typically larger than a single PLIF cage as shown in Figure 1 [5].

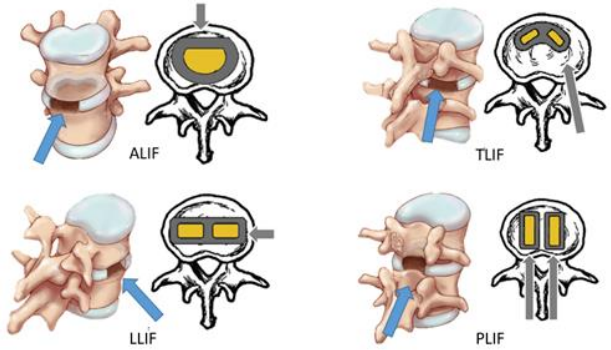

Figure 1. The various surgical approaches to the intervertebral disc space. Arrows show the direction of implantation

LLIF provides a number of benefits over other techniques because of its lateral approach strategy and cage structural characteristics. In this technic, a number of significant anatomical components have been retained, such as facet joints, back muscles, and anterior and posterior longitudinal ligaments. In addition, a minimally invasive method can shorten the length of the procedure or the intraoperative bleeding. Injury risks to the peritoneum, bowels, and great vessels are considerably lower than with the ALIF. The LLIF cage, which has a higher profile and wider width than the TLIF, can indirectly raise the disc height and decompress the neural foramen. Patients with lumbar degenerative kyphosis (LDK) or scoliosis may also benefit from the LLIF cage for the restoration of coronal and sagittal balance.

The materials for the cage can be ceramic, polymeric, or metallic (mainly titanium alloys), though polymer materials are increasingly chosen because of their radio transparency. The most commonly utilized polymeric materials are polyether-ether-ketone (PEEK) [4-7]. Carbon fiber-reinforced polymer (CF-P) material has also been used. The CF-P cages achieved high rates of fusion and good to excellent clinical results, but PEEK has mainly replaced them due to its greater elastic modulus. Recent research has also looked into the development of biodegradable cages using polylactic acid (PLLA)-polyglycolic acid (PGLA) copolymers and poly (L-lactide-coD, L-lactide), which exhibit the required rigidity at the time of implantation with gradual degradation to support bone formation and solid arthrodesis [2]. PEEK (E=3.6 GPa) and Polylactic acid (E=1.5 GPa) have the advantage of having a Young modulus that is far lower than titanium's (E=110 GPa) and considerably closer to that of cortical bone (E= 12 GPa) and vertebral trabecular (E=0.1 GPa). Implants made of stainless steel have an elastic modulus of about 200 GPa. [8-9]. The standard type of LLIF cage has a 6° of lordotic angle and 18 mm of width (Figure 2).

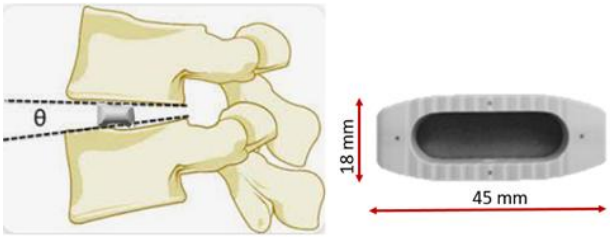

Figure 2. The standard type of LLIF cage [6]

Kim et al [6] studied LLIF cages with greater widths (22 mm and 26 mm) to lower the risk of subsidence in osteoporotic patients. Pimenta et al. [10] compared the 11, 18, and 26 mm XLIF cages, and they suggested that wider cages are biomechanically stable and provided the possibility of using less or even no supplemental fixation for interbody lumbar fusion. Although statements based on the optimum cage design in terms of human anatomy have been reached, design optimization needs to become a focus in order to provide the overall advantages of all fields in the ideal design. Since the subsidence rate varied depending on the type of cages, it should be studied thoroughly. Many studies characterized the compressive strength of different cage designs, especially the ones that are widely used today [11-13]. Despite the increasing clinical use and interest in intervertebral cages, few studies investigated the biomechanical behavior of novel LLIF cage designs in terms of material and cage design optimization [14]. The objective of this study was to compare the compression strength of the LLIF cage-vertebral contact and the immediate three-dimensional changes in flexibility brought on by cage insertion. This study aims to design a novel LLIF cage, which has larger anterior-posterior widths, and to explore the potential benefits of the cage with less stiffness than current cage devices.

2 Material and methods

2.1 Designing of the LLIF spine cages

The software CATIA V5R21 (Dassault Systèmes, Vélizy-Villacoublay, France) was used to create solid representations of the L3- L4 vertebrae and LLIF cages. This lumbar spine and the intervertebral disc were derived from open-source cadaver CT scan data. The patient was approximately 40 years old when the scan was taken. Between the superior surface of L3 and the inferior surface of L4, the spinal cage was placed. The size of the cage is dependent on this L3-L4 typical distance between two neighboring vertebrae in the adult lumbar area. As shown in Figure 3, 3D models of multiple alternative LLIF spine cages were designed based on the L3-L4 vertebrae model.

The cage height was chosen to preserve disc space and lordosis according to the L3-L4 model. The center of an interbody device is usually hollow and is often filled with bone grafts to enhance fusion [15]. The outer shape and inner porous core structure of these cages were designed. Two different cage structures, which have a larger footprint, were investigated as shown in Figure 4.

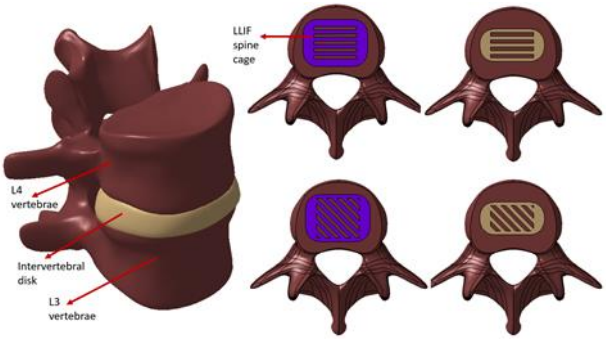

Figure 3. LLIF spinal cage designs

Figure 4a shows the straight inner core design with 2 mm square beam structures. Figure 4b displays the core design with 2 mm square beam structures tilted 45 degrees. The designed cage designs had a constant 2.6 ° lordotic angle and 36 mm length. While the straight cage width of 18 mm design has a volume of $3.308x10^{-6}$ m^3, the 45-degree tilted design has a volume of $3.54x10^{-6}$ m^3. The straight cage width of 26 mm has a volume of $5.62x10^{-6}$ m^3, while the 45-degree tilted cage design has a volume of $4.93x10^{-6}$ m^3.

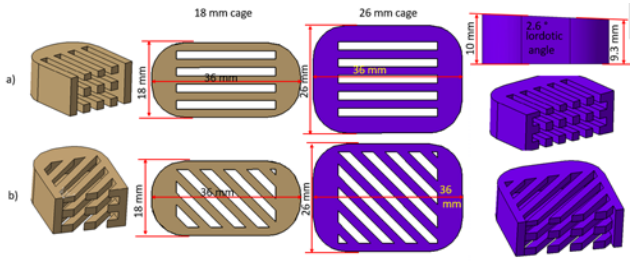

Figure 4. LLIF spinal cage designs

Porosity is calculated from Equation 1 [16].

$$P\ (\%) = \left(1 - \frac{Vf}{Vt}\right) x100 \qquad (1)$$

Where Vf is the design volume of the cage, and Vt is the bulk volume of the CAD model. The porosity values of the spinal cages are displayed in Table 1.

Table 1. The porosity of the designed scaffolds

Cage	18 mm width	26 mm width
Straight	42.43 %	40.09 %
45 degree tilted	39.96 %	41.68 %

2.2 Finite element analysis

The model's material properties were considered to be homogeneous and isotropic and chosen from the previous research (Table 2). The vertebral body was divided into two parts: cortical bone, and cancellous bone. The cortical bone had a 1.0 mm thickness which is in agreement with [17]. The intervertebral disc consists of annulus fibrosus, annulus matrix, and nucleus pulposus. However, the disc was regarded as having annulus matrix characteristics for the analysis because the primary purpose of the study was not to model the disk. It was only planned to make an overall comparison of the results with the disc material properties.

The influence of the different cage materials (PEEK, PLA, Titanium, stainless steel) is also examined in this study.

Table 2. Material properties used in the Finite element model of the lumber spine

Material Properties	Young Modulus, (MPa)	Poisson ratio	Density (kg/m^3)	Reference
Cortical bone	12000	0.3	2060	[18,19]
Cancellous bone	100	0.2	1300	[19,20]
Intervertebral disc	4.2	0.45	1060	[21]
Cage (PEEK material)	3620	0.39	1320	[22]
Cage (PLA material)	1459	0.4	1280	[22]
Cage (annealed, Ti-6A-14V)	111200	0.3387	4429	[23]
Cage (Stainless Steel material)	193000	0.3	8000	[24]

Finite element (FE) analysis was carried out utilizing ANSYS Workbench 2022, R2 (Canonsburg, Pennsylvania, U.S.). The basic physiological movements of L3 and L4—compression, axial rotation, and lateral bending—are taken into consideration in the analysis. First, a static, axial compressive force along the x-axis of 730 N was applied uniformly throughout the surface of L3 vertebrae, fixing L4 vertebrae (Load case 1). The highest in vivo force measured in the lumbar spine of a patient rising from a chair was used to determine the load [25]. Secondly, the L3 vertebra was subjected to a 7.5 Nm moment (Load case 2). The load was applied similarly to the experimental study of Song et al [26]. Finally, a 15 Nm moment was applied to the cage's mass center to imitate bending force (Load case 3). All the boundary conditions are shown in Figure 5. The loads' magnitudes were determined using numerical simulations of the loads acting on the lumbar portions of the spine [27]. The facet contact was set to a surface-to-surface frictionless interaction. The other component's contact condition was taken to be a bonding contact in order to prevent the separation of the parts when a load was applied.

The Static Structural module of the ANSYS Workbench was used to generate the mesh for the FE study. A sensitivity analysis of the mesh was performed to determine the element size. The FE model was meshed using 3D tetrahedral elements. Automatic meshing was applied to the L3-L4 model with resolution 7. The minimum element quality for the L3-L4 model without the cage was around 0.767. For the cages, the body sizing meshing method was applied and 0.4 mm element size was set for each cage (Figure 5). The minimum element quality for the 18 mm width straight cage, 18 mm width 45° tilted cage, 26 mm width straight cage, and 26 mm width 45° tilted cage was around 0.150, 0.266, 0.237, and 0.154, respectively.

To assess the load distribution in the model and to compare with experimental observations, the von Mises (distortional) stress and strains for each of these elements were recorded.

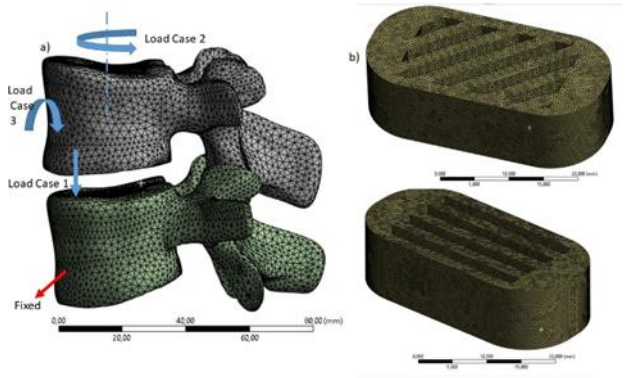

Figure 5. The meshing of a) L3-L4 model, b) cage

3 Results and discussions

The stress and strain distribution on the L3-L4 model with spinal cages was taken based on the FE analysis to better understand the stress behavior and the influence of the cage geometry on both vertebral bones. In Figure 6 von-Mises stress results of the L3-L4 model with 18 mm tilted cage for each load case are shown. Figures 7, 8, and 9 show the von-Mises stresses to better understand the stress distribution for the PLA cages between the vertebrae. The human intervertebral disc had around 3.26 MPa [28]. It is aimed to have similar values to the human body parts. The 18 mm cage designs had higher von-Mises stress values than the 26 mm cage designs. This is because cages with greater widths disperse load across a larger region of the vertebrae, reducing the risk of subsidence in osteoporotic patients. This could be because the wide cage's wider footprint can cover more of the vertebral body's peripheral region, offering better mechanical support and more resistance to subsidence. Wider cages may also increase stability by blocking motion over standard 18 mm cages [29,30]. The wide design and inner core structure maximize surface area for fusion and it has a large opening for graft insertion within the disc space. Moreover, the novel designs provided sufficient but not excessive strength and effectively transmit strain energy to the regenerated bone. The design can have sufficient space for the delivery of biologics and bone ingrowth and can transfer loads seamlessly from the designed cage to newly grown bone tissue [15].

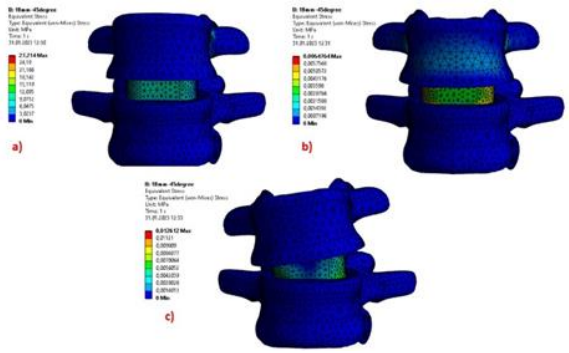

Figure 6. Von-Mises stress results of L3-L4 model with 18 mm tilted cage (a) Load case 1, (b) Load case 2, (c) Load case 3

The von-Mises stress value on the 26 mm tilted cage was higher than the 26 mm straight cage. This can be explained by the variation of the porosities of the cages. According to Table 1, the 26 mm straight cage had a porosity value of 40% whereas the 26 mm tilted cage had a value of 42%. Because of the lower porosity, stress should be lower. Higher porosity causes stress concentration around the cage and decreases the mechanical strength [30].

The stress and strain distributions on the L3-L4 model with the designed spinal cages with the load cases 1, 2, and 3 were taken based on the FE analysis and are shown in Figures 7, 8, and 9 and listed in Table 3. The intervertebral disk was also analyzed in order to compare the results with it; it had an equal von-Mises stress of 14.957 MPa and a strain value of 0.967 mm/mm. The trend of the stress decreased as the width of the cage increased and comparing the tilted to straight cage designs, the equivalent stress for cages of the same width decreased. This is because a wider cage results in an increase in segmental stiffness in all loading directions. A stiffer segment in extension and lateral bending is produced by a longer and wider cage [32]. Moreover, the subsidence resistance is increased with a wider cage. Subsidence is less likely to occur with better normal stress distribution, while migration is less likely to occur with better shear stress distribution. Reduced maximum equivalent stresses and strains will result in better stress distribution inside the cage, which will reduce the probability of subsidence and migration [4].

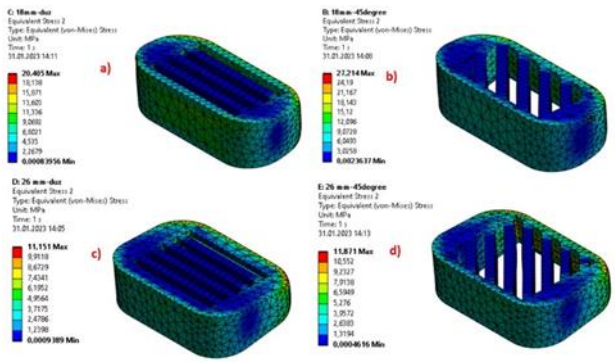

Figure 7. Load case 1 von-Mises stress distribution on the cage bodies (a) 18 mm straight, (b) 18 mm tilted, (c) 26 mm straight, (d) 26 mm tilted

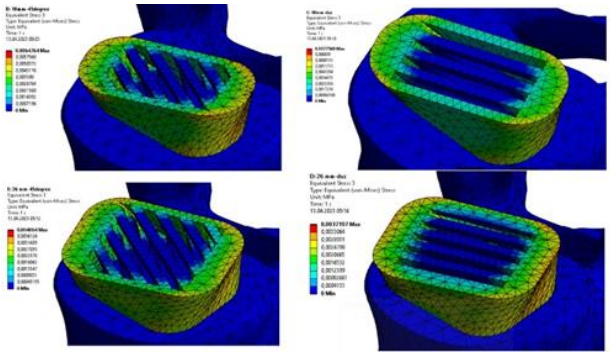

Figure 8. Load case 2 von-Mises stress distribution on the cage bodies (a) 18 mm straight, (b) 18 mm tilted, (c) 26 mm straight, (d) 26 mm tilted

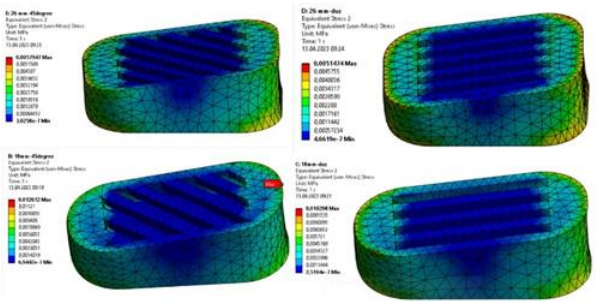

Figure 9. Load case 3 von-Mises stress distribution on the cage bodies (a) 18 mm straight, (b) 18 mm tilted, (c) 26 mm straight, (d) 26 mm tilted

The equivalent stress showed a similar pattern in load case 1, at the 26 mm straight and tilted cages between lumbar 3 and 4. Due to the cross-sectional cage area in the direction of 750 N loading (Load case 1) resulted in close surface areas for straight and tilted cages, which were $6.417x10^{-4}$ m^2 and $6.181x10^{-4}$ m^2, respectively.

This mismatch results from the fact that uniform properties for the bone structures were taken into account in this investigation due to a lack of material data.

When the spine is flexed or rotated, the stress exerted on the cage is enlarged, supporting results found in clinical studies. Most ligaments are stretched as the vertebral body rotates. The distribution of the stress value for the designed 26 mm cage model is similar to that of the intervertebral disc. However, there is a substantial difference in the displacement values between these two. The shifting range of stress and the intervertebral disc's influence on stress are both the smallest for rotational and extension movements. We can therefore come to the conclusion that intervertebral disc diseases are not primarily caused by rotational and extension movements which is in agreement with [33].

Previous research has shown that the cage between vertebrae shouldn't sag by more than 2 millimeters [19]. For each load case, it is maintained. In each geometry, the subsidence is small. Overall, torsion movement is associated with the lowest subsidence in all geometric designs. Since the cage is in direct contact with the bone area during load case 1, the cartilage is most likely to be destroyed.

Additionally, the core section area displays a rise with wide cage geometries that reduces subsidence for the cage used in the body. In addition, increasing the bone graft gap causes the fusion rate to increase and the optimized cage to more successfully endure stress and subsidence [19].

The cage material also has a significant impact on both its final cost and functionality. The mechanical and chemical properties of new materials are being developed to be more compatible with bone. Since the 26 mm straight wide cage gave the best values, this cage has been tested on different materials. In Table 4, the results of various cage materials are displayed. These results demonstrated that the maximum von Mises stress of PEEK and PLA is very close. Titanium and stainless steel are in the range of 306 MPa due to titanium's and stainless steel's higher Young's modulus than bone. It is possible to modify PEEK and PLA cages to provide strength and stiffness that are comparable to cancellous or cortical bone, thereby eliminating overloading risks.

The von-Mises values, as shown in Table 4, are similar to the human disk materials. It is suggested that the spinal movement could be supported by the cage geometry and material.

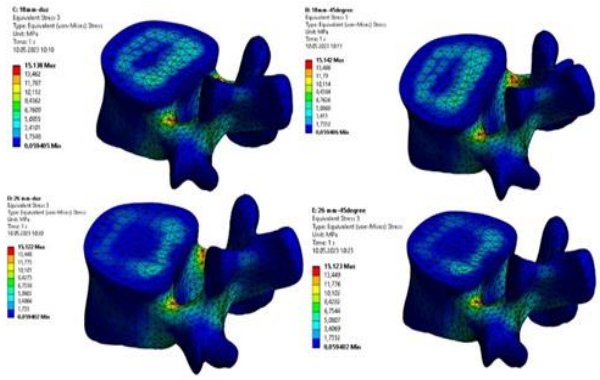

Figure 20. Load case 1 von-Mises stress distribution on the L4 vertebrea (a) 18 mm straight, (b) 18 mm tilted, (c) 26 mm straight, (d) 26 mm tilted

Figure 10 illustrates the investigation of the equivalent stress experienced by L4 vertebra in load case 1, considering different widths and inner core designs of the placed spinal cage. Von-Mises stress acting on the L4 vertebra was higher in the 18 mm cage designs than the 26 mm cage designs. This is due to the fact that wider cages distribute weight over a broader area of the vertebrae, lowering the likelihood of subsidence in individuals who are osteoporotic. Greater mechanical support and increased resistance to subsidence are provided by the wide cage's bigger footprint, which can encompass more of the vertebral body's periphery [29,30]. The equivalent stress showed a similar pattern when 26 mm straight and tilted cages were placed at the L4 vertebrae in load case 1. With the human intervertebral disc, the max Von-Mises stress acting on L4 was determined as 14,957 MPa.

Table 3. ANSYS analysis results of the L3-L4 model with the designed cages

	Load Case 1		Load Case 2		Load Case 3	
PLA Cage	Equivalent von-Mises stress (MPa)	Equivalent Elastic Strain (mm/mm)	Equivalent von-Mises stress (MPa)	Equivalent Elastic Strain (mm/mm)	Equivalent von-Mises stress (MPa)	Equivalent Elastic Strain (mm/mm)
Disk	14.957	0.967	0.005	$521x10^{-6}$	0.004	0.001
18 mm-straight	20.405	0.014	0.008	$5.319x10^{-6}$	0.010	$7.069x10^{-6}$
18 mm- tilted	27.214	0.019	0.006	$4.492x10^{-6}$	0.013	$8.660x10^{-6}$
26 mm- straight	15.122	0.008	0.004	$2.734x10^{-6}$	0.005	$3.528x10^{-6}$
26 mm-tilted	15.123	0.008	0.004	$2.973x10^{-6}$	0.006	$3.975x10^{-6}$

Table 4. ANSYS analysis results of the 26 mm- straight cage in different materials

	Load Case 1		Load Case 2		Load Case 3	
26 mm-straight Cage	Equivalent von-Mises stress (MPa)	Equivalent Elastic Strain (mm/mm)	Equivalent von-Mises stress (MPa)	Equivalent Elastic Strain (mm/mm)	Equivalent von-Mises stress (MPa)	Equivalent Elastic Strain (mm/mm)
Disk	14.957	0.967	0.005	$521x10^{-6}$	0.004	0.001
PLA	15.122	0.007764	0.0037	$2.734x10^{-6}$	0.00511	$3.528x10^{-6}$
PEEK	15.122	0.003385	0.0038	$1.124x10^{-6}$	0.00514	$1.413x10^{-6}$
Titanium	305.99	0.034292	0.006	$0.211x10^{-6}$	0.007	$0.071x10^{-6}$
Stainless Steel	306.15	0.034348	0.007	$0.211x10^{-6}$	0.009	$0.05x10^{-6}$

4 Conclusions

In this work, the effect of varying spinal cage width design has been studied using FE models of the vertebral bone. The load was simulated to the lumbar L3-L4 segment using the finite element method. In addition, the stress distributions in these PLA, PEEK, stainless steel, and titanium cages with the same designs were then compared. This study aims to improve the LLIF spine cage, which can adjust to the direction and small size of insertion that match the spine size of patients. A spinal cage, which had a larger cross-sectional area, was designed and stresses were decreased. The results of this study suggest that polymer materials, as opposed to metallic ones, may help to reduce the incidence of subsidence. Vertebral endplate stresses were reduced by the PLA straight 26 mm cage, which also kept implant, stresses below the threshold for axial compressive loading. Cages with greater widths disperse load across a larger region of the vertebrae, reducing the risk of subsidence because of the cage's wider footprint. However, the most important factor in determining the maximum cage width would be the risk of brain injury during insertion.

Conflict of interest

The author declares that there is no conflict of interest

Similarity rate (iThenticate): %19

References

[1] A. Faadhila, S.F. Rahman, Y. Whulanza, S. Supriadi, J.Y. Tampubolon, S.I. Wicaksana and A.H. Abdullah, Design of a Transforaminal Lumbar Interbody Fusion (TLIF) Spine Cage. International Journal of Technology, 13(8), 1663-1671, 2022. https://doi.org/10.14716/ijtech.v13i8.6152

[2] E. Chong, M. H. Pelletier, R. J. Mobbs and W. R. Walsh, The design evolution of interbody cages in anterior cervical discectomy and fusion: a systematic review. BMC musculoskeletal disorders, 16, 1-11, 2015. https://doi.org/10.1186/s12891-015-0546-x

[3] D. S. Xu, C. T. Walker, J. Godzik, J. D. Turner, W. Smith and J. S. Uribe, Minimally invasive anterior, lateral, and oblique lumbar interbody fusion: a literature review. Annals of translational medicine, 6(6), 1-10, 2018. https://doi.org/10.21037/atm.2018.03.24

[4] S. Choudhury, D. Raja, S. Roy and S. Datta, Stress analysis of different types of cages in cervical vertebrae: a finite element study, Materials Science and Engineering, 912 (2), 022025, 2020. https://doi.org/10.1088/1757-899X/912/2/022025

[5] J. H. Peck, K. D. Kavlock, B. L. Showalter, B. M. Ferrell, D. G. Peck and A. E. Dmitriev, Mechanical performance of lumbar intervertebral body fusion devices: an analysis of data submitted to the Food and Drug Administration. Journal of Biomechanics, 78, 87-93, 2018. https://doi.org/10.1016/j.jbiomech.2018.07.022

[6] S. J. Kim, Y. S. Lee, Y. B. Kim, S. W. Park and V. T. Hung, Clinical and radiological outcomes of a new cage for direct lateral lumbar interbody fusion. Korean Journal of Spine, 11(3), 145-147, 2014 https://doi.org/10.14245/kjs.2014.11.3.145

[7] A. T. Güner ve C. Meran, Ortopedik implantlarda kullanılan biyomalzemeler. Pamukkale Üniversitesi Mühendislik Bilimleri Dergisi, 26(1), 54-67, 2020. https://doi.org/10.5505/pajes.2019.46666

[8] H. T. Hee and V. Kundnani, Rationale for use of polyetheretherketone polymer interbody cage device in cervical spine surgery. The Spine Journal, 10(1), 66-69, 2010. https://doi.org/10.1016/j.spinee.2009.10.014

[9] M. van Dijk, T. H. Smit, S. Sugihara, E. H. Burger and P. I. Wuisman, The Effect of Cage Stiffness on the Rate of Lumbar Interbody Fusion: An: In Vivo: Model Using Poly (L-Lactic Acid) and Titanium Cages. Spine, 27(7), 682-688, 2002. https://doi.org/10.1097/00007632-200204010-00003

[10] L. Pimenta, A. W. Turner, Z. A. Dooley, R. D. Parikh and M. D. Peterson, Biomechanics of lateral interbody spacers: going wider for going stiffer. The Scientific World Journal, 2012.381814. 2012. https://doi.org/10.1100/2012/381814

[11] B. Jost, P. A. Cripton, T. Lund, T. R. Oxland, K. Lippuner, P. Jaeger and L. P. Nolte, Compressive strength of interbody cages in the lumbar spine: the effect of cage shape, posterior instrumentation and bone density. European Spine Journal, 7, 132-141, 1998. https://doi.org/10.1007/s005860050043

[12] M. Krammer, R. Dietl, C. B. Lumenta, A. Kettler, H. J. Wilke, A. Büttner and L. Claes, Resistance of the lumbar spine against axial compression forces after implantation of three different posterior lumbar interbody cages. Acta neurochirurgica, 143, 1217-1222, 2001. https://doi.org/10.1007/s007010100017

[13] T. G. Lowe, S. Hashim, L. A. Wilson, M. F. O'Brien, D. A. Smith, M. J. Diekmann and J. Trommeter, A biomechanical study of regional endplate strength and cage morphology as it relates to structural interbody support. Spine, 29(21), 2389-2394, 2004. https://doi.org/10.1097/01.brs.0000143623.18098.e5

[14] T. Lund, T. R. Oxland, B. Jost, P. Cripton, S. Grassmann, C. Etter and L. P. Nolte, Interbody cage stabilisation in the lumbar spine: biomechanical evaluation of cage design, posterior instrumentation and bone density. The Journal of bone and joint surgery. British volume, 80(2), 351-359, 1998. https://doi.org/10.1302/0301-620x.80b2.7693

[15] H. Kang, S. J. Hollister, F. La Marca, P. Park and C. Y. Lin, Porous biodegradable lumbar interbody fusion cage design and fabrication using integrated global-local topology optimization with laser sintering. Journal of biomechanical engineering, 135(10), 101013, 2013. https://doi.org/10.1115/1.4025102

[16] R. Sala, S. Regondi and R. Pugliese, Design Data and Finite Element Analysis of 3D Printed Poly (ε-Caprolactone)-Based Lattice Scaffolds: Influence of Type of Unit Cell, Porosity, and Nozzle Diameter on the Mechanical Behavior. Eng, 3(1), 9-23, 2022. https://doi.org/10.3390/eng3010002

[17] H. Zhang, D. Hao, H. Sun, S. He, B. Wang, H. Hu and Y. Zhang, Biomechanical effects of direction-changeable cage positions on lumbar spine: a finite element study. American Journal of Translational Research, 12(2), 389-396, 2020. https://www.ncbi.nlm.nih.gov/pmc/articles/PMC7061850/

[18] H. Ding, L. Liao, P. Yan, X. Zhao and M. Li, Three-dimensional finite element analysis of l4-5 degenerative lumbar disc traction under different pushing heights. Journal of Healthcare Engineering, 1322397, 2021. https://doi.org/10.1155/2021/1322397

[19] E. Jalilvand, N. Abollfathi, M. Khajehzhadeh and M. Hassani-Gangaraj, Optimization of cervical cage and analysis of its base material: A finite element study. Proceedings of the Institution of Mechanical Engineers, Part H: Journal of Engineering in Medicine, 236(11), 1613-1625, 2022. https://doi.org/10.1177/09544119221128467

[20] S. Dayanand, B. R. Kumar, A. Rao, C. CV, M. B. Khot and H. Shetty, Finite element modelling and dynamic characteristic analysis of the human CTL-Spine. Vibroengineering Procedia, 30, 116-120, 2020. https://doi.org/10.21595/vp.2020.21390

[21] R. A. SI, C. CV and P. Goplani, Fracture strength estimation of L3-L4 intervertebral disc using FEA. Vibroengineering Procedia, 27, 67-72, 2019. https://doi.org/10.21595/vp.2019.20976

[22] M. H. Jalil, M. H. Mazlan and M. Todo, Biomechanical comparison of polymeric spinal cages using Ct based finite element method. International Journal of Bioscience, Biochemistry and Bioinformatics, 7(2), 110-117, 2017. https://doi.org/10.17706/ijbbb.2017.7.2.110-117

[23] A. Kugendran, L. Mahendran and M. H. bin Jalil, Finite Element Analysis Of Different Spinal Cage Designs For Posterior Lumbar Interbody Fusion. Proceedings of International Exchange and Innovation Conference on Engineering & Sciences (IEICES), 7, 51-57, 2021. https://doi.org/10.5109/4738560

[24] D. Amalraju and A. S. Dawood, Mechanical strength evaluation analysis of stainless steel and titanium locking plate for femur bone fracture. Engineering Science and Technology: An International Journal, 2(3), 381-388, 2012.

[25] L. S. Chatham, V. V. Patel, C. M. Yakacki and R. Dana Carpenter, Interbody spacer material properties and design conformity for reducing subsidence during lumbar interbody fusion. Journal of biomechanical engineering, 139(5), 0510051-0510058, 2017. https://doi.org/10.1115/1.4036312

[26] C. H. Song, J. S. Park, B. W. Choi, J. S. Lee and C. S. Lee, Computational Investigation for Biomechanical Characteristics of Lumbar Spine with Various Porous Ti–6Al–4V Implant Systems. Applied Sciences, 11(17), 8023, 2021. https://doi.org/10.3390/app11178023

[27] T. Serra, C. Capelli, R. Toumpaniari, I. R. Orriss, J. J. H. Leong, K. Dalgarno and D. M. Kalaskar, Design and fabrication of 3D-printed anatomically shaped lumbar cage for intervertebral disc (IVD) degeneration treatment. Biofabrication, 8(3), 035001, 2016. https://doi.org/10.1088/1758-5090/8/3/035001

[28] N. Nishida, F. Jiang, J. Ohgi, M. Fuchida, R. Kitazumi, Y. Yamamura and T. Sakai, Biomechanical Analysis of the Spine in Diffuse Idiopathic Skeletal Hyperostosis: Finite Element Analysis. Applied Sciences, 11(19), 8944, 2021. https://doi.org/10.3390/app11198944

[29] W. Cho, C. Wu, A. A. Mehbod and E. E. Transfeldt, Comparison of cage designs for transforaminal lumbar interbody fusion: a biomechanical study. Clinical Biomechanics, 23(8), 979-985, 2008. https://doi.org/10.1016/j.clinbiomech.2008.02.008

[30] K. Phan and R. J. Mobbs, Evolution of design of interbody cages for anterior lumbar interbody fusion. Orthopaedic surgery, 8(3), 270-277, 2016. https://doi.org/10.1111/os.12259

[31] X. Miao and D. Sun, Graded/gradient porous biomaterials. Materials, 3(1), 26-47, 2009. https://doi.org/10.3390/ma3010026

[32] A. Calvo-Echenique, J. Cegoñino, R. Chueca and A. Pérez-del Palomar, Stand-alone lumbar cage subsidence: A biomechanical sensitivity study of cage design and placement. Computer methods and programs in biomedicine, 162, 211-219, 2018. https://doi.org/10.1016/j.cmpb.2018.05.022

[33] B. Yu, C. Zhang, C. Qin and H. Yuan, FE modeling and analysis of L4-L5 lumbar segment under physiological loadings. Technology and Health Care, 23(s2), S383-S396, 2015. https://doi.org/10.3233/THC-150975.